Slow time scales in a dense vibrofluidized granular material

Andrea Plati[1] and Andrea Puglisi[2]

[1]*Dipartimento di Fisica, Università di Roma Sapienza, P. le Aldo Moro 2, 00185 Rome, Italy*

[2]*Istituto dei Sistemi Complessi–CNR and Dipartimento di Fisica, Università di Roma Sapienza, P. le Aldo Moro 2, 00185 Rome, Italy*

(Received 19 March 2020; accepted 2 July 2020; published 27 July 2020)

Modeling collective motion in nonconservative systems, such as granular materials, is difficult since a general microscopic-to-macroscopic approach is not available: there is no Hamiltonian, no known stationary densities in phase space, and not a known small set of relevant variables. Phenomenological coarse-grained models are a good alternative, provided that one has identified a few slow observables and collected a sufficient amount of data for their dynamics. Here we study the case of a vibrofluidized dense granular material. The experimental study of a tracer, dispersed into the media, showed evidence of many time scales: Fast ballistic, intermediate caged, slow superdiffusive, and very slow diffusive. A numerical investigation has demonstrated that a tracer's superdiffusion is related to slow rotating drifts of the granular medium. Here we offer a deeper insight into the slow scales of the granular medium, and we propose a phenomenological model for such a "secular" dynamics. Based upon the model for the granular medium, we also introduce a model for the tracer (fast and slow) dynamics, which consists in a stochastic system of equations for three coupled variables, and is therefore more refined and successful than previous models.

DOI: 10.1103/PhysRevE.102.012908

I. INTRODUCTION

Granular materials stand as prototypes of physical systems with both important industrial applications and fundamental theoretical challenges [1,2]. When the external perturbation is absent or very weak (and/or sparse in time), a granular medium behaves as an athermal amorphous solid: In this regime, theoretical approaches are scarce and can rarely be compared quantitatively with experiments [3,4]. The situation is different in the case of so-called vibrofluidized regime, i.e., when a continuous external perturbation is applied, for instance by means of vibrating the box that contains the grains, provided that maximum shaking accelerations are much larger than gravity acceleration [5,6]. Actually such a regime can be separated into several different phases, depending upon the amount of grains in the container (typically measured through the number of layers at rest, or the average density/packing fraction) and the shaking parameters [7,8]. In the most dilute and agitated phase, the so-called granular gas, quantitative predictions are obtained through granular kinetic theory [2] and granular hydrodynamics [9,10]. Those are bottom-up theories where macroscopic/average quantities, such as the transport coefficients, can be deduced from the knowledge of the laws of interaction among the single grains, with the assumption (true in the dilute Grad-Boltzmann limit) of molecular chaos, or its revised version called the Enskog approximation [2,9,11–13]. In recent decades, kinetic theory of molecular systems has made important progress toward a quantitative understanding of the liquid phase [14,15], with success in explaining certain aspects of slow relaxations in supercooled liquids [16,17]. A similar approach has been applied to vibrofluidized granular systems in order to obtain some predictions in nondilute phases [18,19]. This approach—based upon a granular adaptation of mode coupling theory (MCT) [17]—reproduces the qualitative behavior of the relaxation of density correlations in the system, with the possibility of marking a glass transition where relaxation times diverge: at the qualitative level, everything appears similar to the molecular (nondissipative) case. The diffusional properties of a tracer are also qualitatively similar to molecular liquids, with the standard ballistic → arrested → diffusive scenario for the mean-squared displacement. Rheological properties and the typical thinning-thickening scenario are also explained fairly well with this approach, even if experiments may offer more complex pictures [20].

Experiments in dense vibrofluidized granular liquids in a cylindrical geometry (see Fig. 1) have shown the existence of a complex dynamical scenario with collective phenomena occurring along time scales larger than the cage time scale [21,22]. The cylindrical geometry enhances the possibility of observing such time scales: A cylinder implies the existence of a direction of motion—the rotational one—with an infinite horizon, i.e., without obstacles (only subject to friction). The slow collective dynamics determines two observable phenomena: the superdiffusion (SD) for the dynamics of a tracer immersed in the granular medium [21], and persistent rotational motion (PR) of large parts of the granular medium [22]: both phenomena—strictly correlated—appear when the density is increased and/or the steady vibrofluidization is reduced, and they take place over time scales in the range of 10–10^3 s, depending on the packing fraction and shaking parameters, while interactions occur on time scales of 10^{-3}–10^{-2} s. Interestingly, these unprecedented SD and PR are superimposed to the usually observed fast phenomena occurring over small and medium time scales, such as subcollisional ballistic motion and transient dynamical arrest due to caging. Such persistent motion is not accounted for by the aforementioned granular mode coupling theory, since velocities are factored out in that theory.

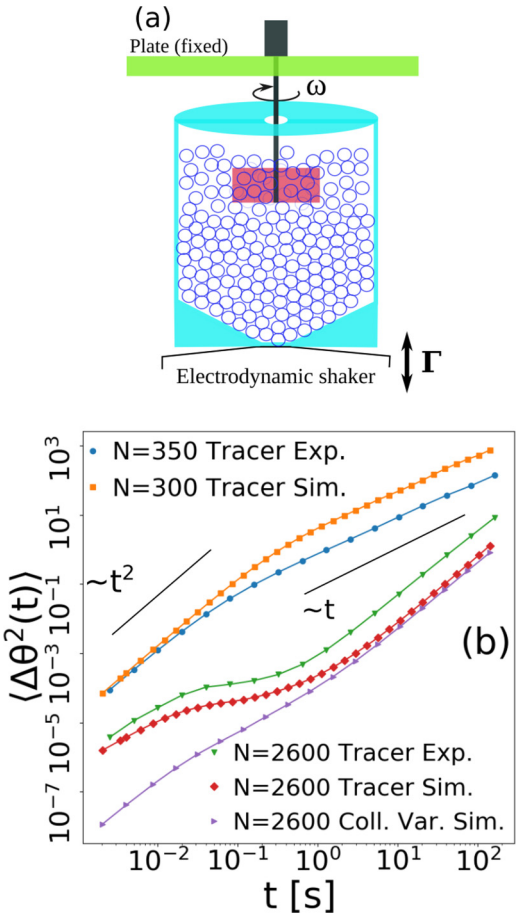

FIG. 1. (a) Setup of the experiment and of the simulation. (b) mean-squared displacements of the tracer (in experiments and simulations) and of the collective rotation of the granular medium (only simulations; see Sec. IV for the definition). $\Gamma = 39.8$ for all the cases shown.

The rotational experiments are not unique—in the context of granular materials—to show some kind of collective motion occurring over very long time scales. A long history of slow convective phenomena exists in regimes where the external vibration is exceedingly weak (below the gravity threshold) [23,24], but we consider those cases substantially different from the case considered here, since they display basically *only* long time scales (no fast phenomena are present). More recently, a series of vibrofluidized experiments has revealed the so-called "low-frequency oscillations" (LFO) [25,26], with frequencies below 1 Hz, superimposed to standard fast relaxational behavior. LFO and SD/PR phenomena occur over different ranges of frequency (LFO close to 1 Hz, SD/PR close to 0.1 Hz), and their connection is still to be analyzed.

It is also interesting to compare the slow collective motion seen in these granular experiments with similar phenomena observed in models and experiments with active matter, for instance in dense populations of bacteria [27,28] and sperms [29], or even within the dynamics of a single flagellum [30].

In this paper, with the help of discrete-element simulations reproducing the original experiment in [21], we aim to elucidate some phenomenological stochastic models with few coarse-grained variables that are able to describe the SD and PR phenomena [31]. These models are an extension and improvement over a previous one proposed in [32], which was built to reproduce only the SD tracer behavior: The limitations of that model are that it is not entirely coherent with the observed tracer power spectra and does not describe the granular medium (i.e., it cannot account for PR). These models share minimality (in the spirit of Occam's razor). In fact, they include only linear couplings and additive independent noises, allowing for an exact analytical treatment: their goal is to characterize the existence of many time scales in the system, and for this purpose nonlinearity is not a crucial ingredient. A more general (not limited to linear coupling) Langevin approach has also been considered by applying a Langevin modeling recipe to the experimental data [33]. Linearly coupled models have been used before in granular modeling: For instance, they are able to characterize the failure of the fluctuation-dissipation relation for the dynamics of a tracer in certain models [34,35], but they have shown certain limitations when compared with experiments [36]. Linear modeling used for the purpose of quantifying nonequilibrium features has also been used recently in the single-flagellum dynamics of active particles [30].

The paper is organized as follows. In Sec. II we give a brief account of the existing stochastic models for this particular granular setup. In Sec. III the ingredients of the simulations are explained. In Sec. IV we show how the collective rotation of the granular medium is well reproduced by the superposition of two *independent* collective variables obeying linear Langevin equations with well-separated time scales. In Sec. V we build upon the previous observation and describe the motion of a rotating tracer as a third rotating variable coupled to the granular medium, resulting *de facto* in a three-variable model that shows a close adherence to experimental and numerical power spectra. In Sec. VI we make a more extensive comparison of the two models with numerical and experimental data in order to rationalize the dependence of the models' parameters on the physical parameters of the system. A more general discussion of the salient features of the proposed models, together with conclusive perspectives, is given in Sec. VII.

II. EXISTING LANGEVIN MODELS

A simple and old model of diffusion in dense liquids is the so-called itinerant oscillator model, where the tracer is caged in a (harmonic) potential well, whose minimum's position is not fixed but slowly diffuses [37,38]: This model helped in rationalizing spectra from neutron scattering experiments on liquids [39]. If diffusion of the potential minimum is slower than the particle's diffusion inside the well, then the behavior of the tracer's mean-squared displacement (MSD) shows a transient plateau (equivalent to the dynamical arrest or caging) followed by ordinary diffusion. If the dynamics inside the well is underdamped, the first part of the tracer's MSD time dependence is ballistic $\sim t^2$. The after-cage part, however, is always of the ordinary diffusive type $\sim t$ as the tracer is slaved to the dynamics of the minimum's position, which is purely diffusive. The extension of this model proposed in [32] was aimed at obtaining long superdiffusive regimes *after* the cage

time. To obtain this result, an underdamped dynamics was considered also for the position of the well's minimum. Such an extension takes the form of four coupled equations for the angular velocity and position of the rotating tracer, $\omega(t)$ and $\theta(t)$, respectively, and for the angular velocity and position of a collective slow variable, which represents the effect of a large group of particles surrounding the tracer (the cage), $\omega_0(t)$ and $\theta_0(t)$, respectively:

$$I\dot{\omega}(t) = -\gamma\omega(t) - k[\theta(t) - \theta_0(t)] + \sqrt{2\gamma T}\eta(t), \tag{1a}$$

$$I_0\dot{\omega}_0(t) = -\gamma_0\omega_0(t) + k[\theta(t) - \theta_0(t)] + \sqrt{2\gamma_0 T_0}\eta_0(t), \tag{1b}$$

$$\theta(t) = \int_0^t \omega(t')dt', \quad \theta_0(t) = \int_0^t \omega_0(t')dt'. \tag{1c}$$

In the above equations, $\eta(t)$ and $\eta_0(t)$ are independent Gaussian white noises with zero average and unitary variance, namely $\langle\eta(t)\eta(t')\rangle = \delta(t-t')$ and $\langle\eta_0(t)\eta(t')\rangle = \delta(t-t')$. The parameters I and I_0 are the inertia of the tracer and of the surrounding medium, γ and γ_0 are the dissipation felt by the two variables, and T and T_0 are "temperatures" (assuming unitary Boltzmann constant $k_B = 1$); see [35] for a discussion of their physical interpretation. The coupling between the tracer and the collective variable, in this model, is represented by the term $-k[\theta(t) - \theta_0(t)]$, which is linear in the *positions*. With large enough values of I_0, the inertia of the cage, the model—which is analytically solvable—reproduces long-time ballistic superdiffusion.

A problem of this model, however, is its inability to entirely reproduce the velocity power density spectrum (PDS), which is put in evidence in Fig. 2. We recall the definition used here for velocity power spectrum,

$$S(f) = \lim_{t_{\rm TOT}\to\infty} \frac{1}{2\pi t_{\rm TOT}} \left| \int_0^{t_{\rm TOT}} \omega(t) e^{2\pi f i} dt \right|^2 \tag{2}$$

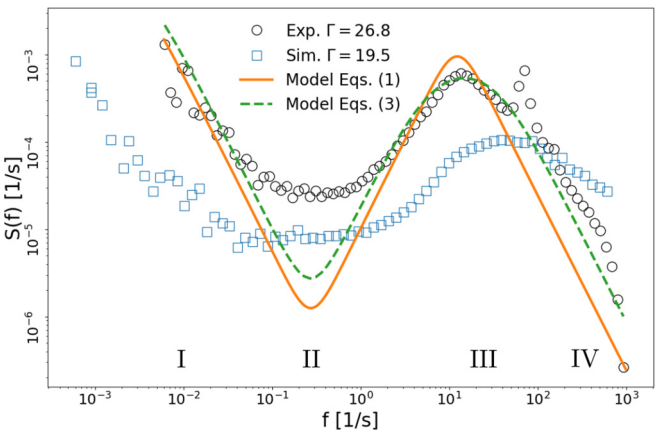

FIG. 2. Comparison of the tracer's velocity power spectra (PDS) in experiments/simulations and the ones predicted (just for the experiments) by Eqs. (1) and (3). The two models fail in reproducing the data in region (II) in the same way. Both experiments and simulations are performed with $N = 2600$. The peak close to 100 Hz seen in the experimental spectrum is directly related to the driving frequency and internal mechanical resonances of the setup; see [21] for details.

(where $t_{\rm TOT}$ is the total simulation time), which is also equivalent to the Fourier transform of the autocorrelation function in the steady state $\langle\omega(t)\omega(0)\rangle$. The experimental/numerical power spectrum—read from high frequencies to low frequencies—shows four main regions (labels are marked in Fig. 2): (IV) at very high frequency a power-law decay (slower than the pure Lorentzian case $\sim f^{-2}$ expected for exponentially decaying velocity autocorrelations), (III) a bumplike peak at smaller frequencies representing the almost periodic oscillations inside a cage, (II) a plateau at even smaller frequencies (suggesting a range of time scales where the process rapidly loses memory), and finally (I) at the smallest observable frequencies (unless day-long experiments are conducted) a decay analogous to the high-frequency one. This decay at very small frequencies is in fact interpreted, in the above model, as the high-frequency decay of a very slow Ornstein-Uhlenbeck process described by $\omega_0(t)$. The most evident discrepancy between theory and experiments/simulations is in the central plateau region (II): the inertial itinerant oscillator model is not able to reproduce it.

A second attempt to obtain a meaningful Langevin model for the angular velocity of the rotating tracer has been done in [33]. Its advantage is that it is the result of a general constructive method of Markovian model-building based upon the experimental data [the experimental time series of $\omega(t)$] and some guess about other possibly relevant variables (when data present non-Markovian character, other variables must be identified in order to obtain a proper Markovian embedding [31]). In such a method, one is also able to verify that the chosen variables are consistent with the Markovian hypothesis. Such an advantage results in a more compact model, with a smaller number of parameters:

$$\dot{\omega}(t) = -A_1\omega(t) - A_2[\theta(t) - \theta_0(t)] + \sqrt{2B}\eta(t), \tag{3a}$$

$$\dot{\omega}_0(t) = -A_0\omega_0(t) + \sqrt{2B_0}\eta_0(t), \tag{3b}$$

$$\theta(t) = \int_0^t \omega(t')dt', \quad \theta_0(t) = \int_0^t \omega_0(t')dt', \tag{3c}$$

where $\eta(t)$ and $\eta_0(t)$ are Gaussian noises with unitary variance. This model is a particular limit of the model guessed in [32], where the term $k[\theta(t) - \theta_0(t)]$ is negligible with respect to the other terms in Eq. (1b): indeed with the present definition, ω_0 evolves with a slow dynamics that does not admit fluctuations on the fast time scale of θ_1, so that such a term is necessarily negligible. All other parameters are strictly related to the parameters of the model in Eq. (1): A_0, A_1, A_2, B, and B_0 should be directly compared with γ_0/I_0, γ/I, k/I, $\gamma T/I^2$, and $\gamma_0 T_0/I_0^2$, respectively. This model well reproduces the mean-squared displacement of the tracer with its final superdiffusive part, while its comparison with the power spectrum is unsatisfying in the central part, as in [32]; see Fig. 2.

Models in Eqs. (1) and (3) both involve two independent white noises, but they are nevertheless a three-dimensional linear model in which the Markovian vector is $X(t) = \{z(t), \omega(t), \omega_0(t)\}$ with $z(t) = \theta(t) - \theta_0(t)$. One may wonder if it is possible to obtain satisfying results with a two-variable linear model. We know from the data that a minimum request is a PDS with two stationary points (a minimum and a

maximum) for $f > 0$. In the Appendix we show that this kind of functional form is not compatible with the most general form for a two-variable linear model. In view of this, using a three-variable model is an unavoidable choice if one wants to reproduce the experimental data through stochastic linear models.

III. MICROSCOPIC MODEL

Simulations of the granular experiments are implemented through the LAMMPS package with its module dedicated to granular interactions [40]. LAMMPS is an optimized package that solves the molecular-dynamics equations of motion and in our case incorporates the interactions of discrete elements methods to treat macroscopic (nonmolecular) particles such as the spherical grains of the experimental setup. Specifically, all interactions among the bodies in the simulation, including interactions with the boundaries representing the experimental box, obey the Hertz-Mindlin model [41–43]: The latter is a soft potential that takes into account normal and tangential forces, both composed of elastic and dissipative contributions. Thus, our particles are spheres of mass m_i, radius R_i, and momentum of inertia $I_i = \frac{2}{5} m_i R_i^2$ with spatial coordinates $\vec{r}_i$ that travel with translational velocities $\vec{v}_i$ and rotational velocities $\vec{\omega}_i$. We specify that the flat boundaries of the box are considered as spheres with infinite mass and radius. When centers of mass of two particles are closer than the sum of their radii, a collision takes place, which is the only situation in which the interaction forces are nonzero: in that case, particles i and j compenetrate to each other, and a relative velocity at the surface of contact is defined as $\vec{g}_{ij} = (\dot{\vec{r}}_i - \vec{\omega}_i \times R_i \vec{n}) - (\dot{\vec{r}}_j + \vec{\omega}_j \times R_j \vec{n})$, where $\vec{n} = (\vec{r}_i - \vec{r}_j)/|\vec{r}_i - \vec{r}_j|$; we call $\vec{g}_{ij}^N$ and $\vec{g}_{ij}^T$ the two projections, respectively normal and tangential, to this surface of contact. Now the equations of motion read

$$\dot{\vec{g}}^N = \vec{F}^N / m^{\text{eff}}, \tag{4a}$$

$$\dot{\vec{g}}^T = \frac{7}{2 m^{\text{eff}}} \vec{F}^T, \tag{4b}$$

where $m_{ij}^{\text{eff}} = m_i m_j/(m_i + m_j)$ while $\vec{F}_{ij}^N = \vec{n}(\vec{n} \cdot \vec{F}_{ij})$ and $\vec{F}_{ij}^T = \vec{F}_{ij} - \vec{F}_{ij}^N$ are, respectively, the normal and tangential component of the force $\vec{F}_{ij}$ between the particles. Both of these contributions are made of an elastic and a dissipative term, tuned by coefficients that depend upon the properties of the specific modeled material. To be more compact, we avoid writing here the full form of these terms, reported and explained in detail in the supplemental material of our previous study [22]. In the same reference, it is possible to find also the specific numerical values used to tune our simulations. The simulation setup mimics fairly well the experimental setup of [21] with all its specific components and materials as the cylindrical box with the conical base and the blade used as an intruder. The good quantitative agreement between the experimental and the numerical observations for the intruder has been shown in [22] (see also Fig. 1 here). In the same paper, simulations without the blade have also been performed in order to study the collective motion of the granular medium, inaccessible in the experiments. These studies confirmed that the PR phenomenon displayed by the granular medium is not affected by the presence of the tracer. Nevertheless we specify here that, except when explicitly declared, all the data relative to the collective motion shown in this paper (see Ω defined in the next section) come from simulations performed *without* the blade. To conclude this section, we mention that during the present numerical study an error in the source code of LAMMPS has been found [44]. In particular, the tangential force during the collision was always applied at the surface of the particles (i.e., at a distance R_i from the center), and this naturally led to an unphysical resultant torque during contact. This error is actually critical from a physical point of view because it breaks the conservation of the total angular momentum expected in internal (sphere-sphere) interactions. Nevertheless, we have corrected the code and run all the simulations again verifying that this error does not affect our old and new results in a significant way. Moreover, from the LAMMPS stable release of 5 June 2019 the granular module has been updated and the error fixed [45].

IV. COLLECTIVE VARIABLE (TWO TIME SCALES)

The results presented in [22] demonstrate that the SD phenomenon displayed by the rotating tracer is a direct consequence of the PR phenomenon exhibited by the granular medium: While on small time scales the rotating tracer has its own dynamics with short free flights and rapid bounces against the boundaries of a local cage of surrounding grains, on long time scales the tracer is dragged by a persistent collective rotation of the surrounding medium. Such a medium rotation is measured through a global angular velocity defined as

$$\Omega(t) = \frac{1}{N} \sum_{i=1}^{N} \dot{\theta}_i(t), \tag{5a}$$

$$\theta_i(t) = \arctan\left(\frac{y_i(t)}{x_i(t)}\right), \quad \dot{\theta}_i(t) = \frac{[\mathbf{r}_i(t) \times \mathbf{v}_i(t)]_z}{r_i^2}, \tag{5b}$$

where N is the number of granular particles, $\mathbf{v}_i$ is the velocity of particle i, and $\mathbf{r}_i$ is the position of particle i with respect to a coordinate system such that the origin lies on the axis of rotational symmetry of the setup. The time integral of the global angular velocity represents a global absolute angle

$$\Theta(t) = \int_0^t \Omega(t')dt'. \tag{6}$$

Such a variable, when density is increased and vibrofluidization is weakened, exhibits long persistent drifts in both the clockwise and the anticlockwise direction. This implies the appearance of superdiffusion for its mean-squared angle $\langle \Delta\Theta^2 \rangle(t) = \langle [\Theta(t'+t) - \Theta(t')]^2 \rangle \sim t^\beta$ with $\beta > 1$, as seen in Fig. 1. Conversely, the power spectrum of the global angular velocity $\Omega(t)$ shows a power-law decay at very low frequency. We recall that ordinary diffusion ($\beta = 1$) at long times must correspond, in the power spectrum of the velocity, to a plateau at low frequencies. The low-frequency decay is the symptom of persistent motion at long time scales.

In this section, we propose a model for the dynamics of the collective granular rotation. The model is based upon the same principles applied before to the motion of the tracer, i.e., that persistent memory can be reproduced by considering (at least) an auxiliary slow variable. An analysis of the data

TABLE I. Numerical values of the fitted parameters for the collective variable in simulations via Eqs. (10b)–(10d) with $\alpha = 0$ and the tracer in experiments and simulations via Eqs. (11). The first and second rows refer to the same simulation *with* the blade.

	τ_1 (s)	q_1 (s^{-2})	τ_2 (s)	q_2 (s^{-2})	τ (s)	q (s^{-2})	α
Γ=19.5 Tracer Simulations	9.6×10^{-2}	5.7×10^{-3}	1.1×10^{4}	2.0×10^{-2}	7.3×10^{-4}	4.4×10^{-1}	5.0
$\Gamma = 19.5$ Coll. Var. Sim. with blade	5.8×10^{-3}	1.1×10^{-3}	1.1×10^{4}	8.1×10^{-4}			
$\Gamma = 19.5$ Coll. Var. Simulations	5.8×10^{-3}	1.1×10^{-3}	3.1×10^{4}	1.8×10^{-4}			
$\Gamma = 30.6$ Coll. Var. Simulations	1.1×10^{-2}	1.4×10^{-3}	3.9×10^{3}	9.9×10^{-5}			
$\Gamma = 39.8$ Coll. Var. Simulations	1.2×10^{-2}	2.0×10^{-3}	1.2×10^{3}	6.1×10^{-6}			
$\Gamma = 59.8$ Coll. Var. Simulations	1.4×10^{-2}	3.6×10^{-3}	1.1×10^{3}	5.4×10^{-6}			
$\Gamma = 19.5$ Tracer Experiments	1.03×10^{-1}	1.0×10^{-3}	4.6×10^{3}	4.2×10^{-1}	2.8×10^{-3}	4.5×10^{-1}	6.8
$\Gamma = 23.0$ Tracer Experiments	1.06×10^{-1}	1.1×10^{-3}	7.0×10^{3}	5.1×10^{-1}	2.8×10^{-3}	5.1×10^{-1}	5.0
$\Gamma = 26.8$ Tracer Experiments	1.09×10^{-1}	1.2×10^{-3}	2.0×10^{1}	4.7×10^{-3}	3.0×10^{-3}	6.2×10^{-1}	3.7
$\Gamma = 30.6$ Tracer Experiments	1.10×10^{-1}	1.4×10^{-3}	4.0×10^{1}	3.4×10^{-3}	3.3×10^{-3}	7.3×10^{-1}	2.8
$\Gamma = 39.8$ Tracer Experiments	1.11×10^{-1}	2.0×10^{-3}	1.1×10^{1}	2.5×10^{-3}	4.2×10^{-3}	9.5×10^{-1}	2.1

coming from numerical simulations showed, however, that in this particular case the modeling is even easier.

The model we propose for the dynamics of $\Omega(t)$ is the sum of two independent variables, a fast and a slow one. This direct superposition is different from the model in [32] where the tracer's velocity is always (harmonically) coupled to the slow variable, even at small time scales. In that case, the slow variable represents cage dynamics and the coupling describes the natural confining interaction between the cage and the tracer. However, such a cage dynamics is not present in the collective rotation (no cage exists for the rotational mode of the whole granular medium) and therefore there is not a simple mechanism coupling fast and slow motion: at a first level of approximation we can consider them to be decoupled. We choose for simplicity two independent Ornstein-Uhlenbeck (OU) processes with two different characteristic times $\tau_1 = I_1/\gamma_1$ and $\tau_2 = I_2/\gamma_2$ and, in general, two different temperatures T_1 and T_2. In summary, the model is described by

$$\Omega(t) = \Omega_1(t) + \Omega_2(t), \tag{7a}$$

$$I_1\dot{\Omega}_1(t) = -\gamma_1\Omega_1(t) + \sqrt{2T_1\gamma_1}\eta_1(t), \tag{7b}$$

$$I_2\dot{\Omega}_2(t) = -\gamma_2\Omega_2(t) + \sqrt{2T_2\gamma_2}\eta_2(t). \tag{7c}$$

In fact, the model can be rewritten with a smaller number of parameters: the only coefficients that count are τ_i and $q_i = T_i/I_i$ with $i = 1, 2$.

We are in the presence of a sum of two independent variables, therefore the PDS and the MSD are simply the sum of the two individual OU contributions:

$$\langle\Delta\Theta^2\rangle(t) = 2q_1\tau_1 t + 2q_1\tau_1^2\left(e^{-\frac{t}{\tau_1}} - 1\right) + 2q_2\tau_2 t + 2q_2\tau_2^2\left(e^{-\frac{t}{\tau_2}} - 1\right), \tag{8a}$$

$$S(f) = \frac{q_1\tau_1}{\pi[1 + (2\pi f\tau_1)^2]} + \frac{q_2\tau_2}{\pi[1 + (2\pi f\tau_2)^2]}. \tag{8b}$$

Our idea is then to consider one of the two characteristic times much larger than the other ($\tau_2 \gg \tau_1$). To make clear now the meaning of the two variables, we expect the slow component of the collective variable, Ω_2, to behave similarly

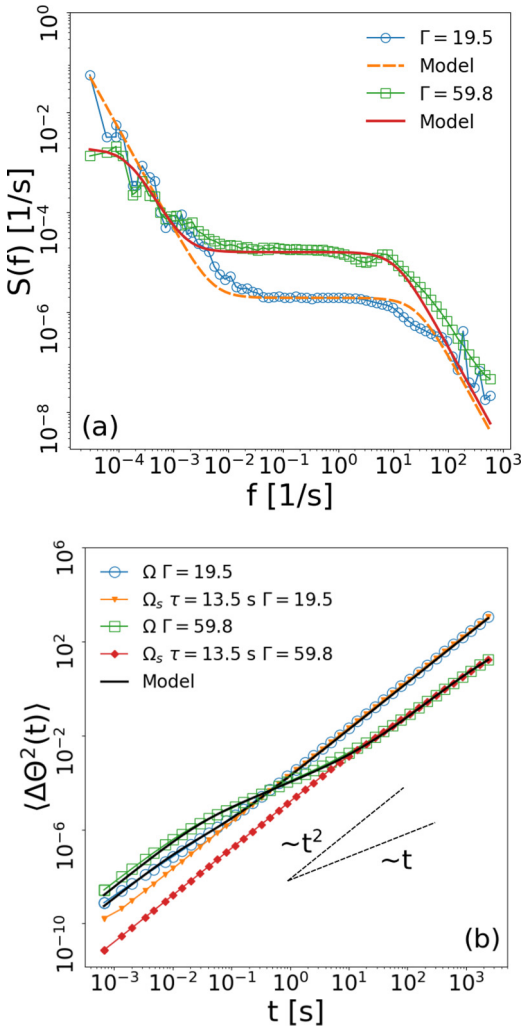

FIG. 3. Collective motion. First comparison between model predictions and numerical data ($N = 2600$, $\Gamma = 19.5$–59.8). MSD and PDS refer to the same signal. The simple model in Eqs. (7) fits well the numerical data for both the PDS and the MSD. The fitted parameters are reported in Table I.

to the filtered variable

$$\Omega_s(t) = \frac{1}{\tau_f}\int_t^{t+\tau_f} \Omega(t')dt', \tag{9}$$

obtained with a moving average of $\Omega(t)$ over a time τ_f such that $\tau_2 \gg \tau_f \gg \tau_1$. To verify this conjecture, we proceed in two ways: first, we try to fit the numerical MSD and PDS via Eqs. (8), and then we show that the superdiffusive part at late times of the collective MSD coincides with the MSD of the filtered variable $\langle \Delta\Theta_s(t)^2\rangle$, where $\Theta_s(t) = \int_0^t \Omega_s(t')dt'$.

In Fig. 3 we show how Eqs. (8) can fit the numerical data for two particular cases of control parameters ($N = 2600$, $\Gamma = 19.5$–59.8), postponing a more systematic analysis to Sec. VI. To obtain the theoretical lines, we first performed a fit of the PDS via Eq. (8b) and then used the parameters inferred in this way also for the MSD [Eq. (8)]. We can see that the model properly predicts the behavior of the two observables. In the PDS there is a good agreement at all the frequency regimes except for the high-frequency decay, where a linear model can only predict a f^{-2} behavior while the data show $f^{-\alpha}$ with $2 > \alpha > 1$. The MSD also exhibits an almost perfect agreement between data and model predictions at all time scales. We conclude that the idea of decomposing the total collective variable into two independent contributions that act at two well-separated time scales is reasonable. Looking at the numerical values of the fitted parameters in Table I, one can can verify that $\tau_2 \sim t_{\rm TOT} \gg \tau_1$.

In Fig. 3(b) we show the MSD of Ω and Ω_s for two values of Γ, one cold case and one hot case at similar density. For the cold case, i.e., at low Γ, we see that $\langle \Delta\Theta(t)^2\rangle$ is ballistic at all times except for the initial ones (the fast component is very weak so the slow one emerges immediately). In the warmer case, we can clearly distinguish the two contributions to the total MSD: the fast one that dominates the first times with its ballistic part and then diffuses, and the slow one that dominates the late times with superdiffusion. Regarding the filtered MSDs, we can see that in both cases it emerges in the total one exactly at the beginning of the superdiffusive regime, at late times. In principle, it is not obvious that the filter used for Ω_s is able to isolate the slow component of a sum of two signals. We can clearly expect that $\langle \Delta\Theta_s(t)^2\rangle$ has to overlap the total MSD for $t > \tau_f$, but how can we be sure that it is really describing the MSD of $\Omega_2(t)$, i.e., the slow component of Ω? We try to answer to this question with Fig. 4, where we study the effect of the filter on two qualitatively different signals for several choices of τ_f. We first discuss the MSD of the collective variable in a dilute case ($N = 300$), where we have an ordinary ballistic-diffusive behavior with just one relevant time scale [22]. We can see that in this case the filter lowers the energy of the ballistic part and stretches the ballistic part up to times $t \sim \tau_f$ where the filtered MSD reunites with the original one. In the dense case (e.g., low Γ), the MSD has the ballistic-diffusive-superdiffusive behavior with two relevant time scales (the fast τ_1 and the slow τ_2 of the aforementioned model), but we can consider a third one τ^* defined as the time for which the slow variable starts to dominate the total MSD (so the time when the late superdiffusion starts, close to τ_2). In this case, the filter acts as in the previous one, but for $\tau_f > \tau^*$ it reaches a kind of saturation and leaves the shape of the MSD unchanged

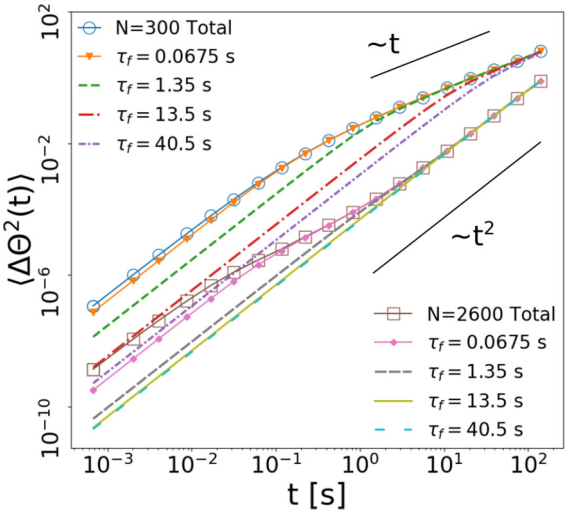

FIG. 4. MSD of the total signals and the filtered ones for several τ_f's and two values of N with fixed $\Gamma = 39.8$.

(see the yellow and cyan-dashed lines that overlap). This implies that for $\tau_f > \tau^*$, the time in which $\langle \Delta\Theta(t)^2\rangle$ and $\langle \Delta\Theta_s(t)^2\rangle$ reunite coincides with τ^* and no longer with τ_f. In view of these last analyses, we can conclude that if in our data a contribution of a slow variable is present, this filter operation tends to isolate it.

To sum up, in this section we have provided evidence of two main facts:

(i) The collective variable behaves as the sum of two independent OU processes with different characteristic times $\Omega(t) = \Omega_1(t) + \Omega_2(t)$.

(ii) A running average $\Omega_s(t) = \tau_f^{-1}\int_t^{t+\tau_f} \Omega(t')dt'$, with τ_f larger than the time τ_1 in which the fast component dominates, successfully isolates $\Omega_2(t)$, i.e., the slow component of Ω.

V. MOTION OF A ROTATING TRACER (THREE TIME SCALES)

Once we have a satisfying model for the collective granular motion, a model for the tracer's motion can be studied on a solid basis, with the aim of improving the model in [32]. The final model for the tracer appears as a system of three equations for three variables (where actually two of them are independent from each other). To build this model, we have considered that the tracer is moving in a complex granular fluid: Such a fluid has two characteristic time scales, as explained in the previous section. The coupling between the tracer and the background granular fluid can be modeled in two different ways: as a conservative interaction that depends upon a relative *position* between the tracer and a representative fluid particle, or as a viscous interaction that depends upon the relative *velocity* between the tracer and the fluid. The first choice was adopted in [32], but our present study convinced us that the second choice gives a better comparison with data. For a viscous interaction we were inspired by [35], where a linear model for a massive granular tracer in a granular fluid (in a planar, not cylindrical, geometry) was considered. The tracer—characterized by velocity $V(t)$—was coupled with the fluid—characterized by local velocity

$U(t)$—through a viscous drag term proportional to $V(t) - U(t)$. Depending on the specific region of the parameter space, this model can reproduce both ordinary Brownian motion and cage effects with the ballistic-caged-diffusive behavior in the MSD and the backscattering peak in the PDS. Therefore, it only lacks the superdiffusion at late times to properly describe the phenomenon of interest here. As we explained in Sec. II, we cannot expect such a complex behavior from a linear model with two variables, therefore we have to insert a third one, trying to be as little artificial as possible. To do so, we leave the equation for the tracer unchanged and complicate the expression of the auxiliary variable making it coincide with the collective variable Ω relative to the subset of the granular particles in the bulk that actually influence the tracer dynamics. This quantity is always modeled by Eqs. (7) and defined by Eq. (5a) but with the mean operation extended just on the aforementioned subset of grains. We expect for it the same *qualitative* behavior (but in general not quantitative) of the global collective variable studied in the previous section: for this reason, we decided not to introduce a new symbol for it.

We end up with a three-variable linear model defined by the following equations:

$$I\dot{\omega}(t) = -\gamma[\omega(t) - \Omega(t)] + \sqrt{2T\gamma}\eta(t), \tag{10a}$$

$$\Omega(t) = \Omega_1(t) + \Omega_2(t), \tag{10b}$$

$$I_1\dot{\Omega}_1(t) = -\gamma_1\Omega_1(t) - \gamma_c\omega(t) + \sqrt{2T_1\gamma_1}\eta_1(t), \tag{10c}$$

$$I_2\dot{\Omega}_2(t) = -\gamma_2\Omega_2(t) + \sqrt{2T_2\gamma_2}\eta_2(t). \tag{10d}$$

Here we see that the bulk collective variable Ω acts as a local velocity field on the tracer whose velocity is $\omega(t)$. At the same time, the fast component of the collective variable Ω_1 is coupled with ω through a viscous constant γ_c. These last two ingredients originate the observed broad cage effect. The slow component Ω_2 is independent of the other variables, and, as suggested by the numerical analysis, it will emerge at late times in the MSD and at small frequency in the PDS. Regarding the physical meaning of the coefficients, we have for each variable an inertia I_i, a viscous coefficient γ_i, and a temperature T_i. We note that the dilute limit (a simple OU process for the tracer) is recovered by sending $\gamma_1/I_1 \to \infty$ and $\gamma_2/I_2 \to \infty$, while the model for the collective variable alone [Eqs. (7)] is obtained by setting $\gamma_c = 0$. As already noted in previous studies [35,46], we recall here that Eqs. (10) are equivalent to a generalized Langevin equation with exponential memory, which is consistent with a typical approximation done for Brownian motion when, at high densities, the coupling of the tracer with fluid hydrodynamics modes, decaying exponentially in time (see [47], Chaps. 8.6 and 9.1), must be taken into account.

From Eqs. (10), exploiting the formalism of the multivariate linear stochastic processes [48], we can compute (see the Appendix) the PDS of the tracer. In Fig. 5 we show a comparison with the experimental and numerical data, finding good agreement in all the frequency regimes. The improvement with respect to the model defined by Eqs. (1) and (3) regards the form of the PDS. In the previous model, the peak and the valley of the PDS are specular, i.e., their position and width depend upon the same combination of parameters, so they cannot be changed independently (Fig. 2). The experimental and numerical PDS show instead that the valley and the backscattering peak are never specular, and in general this is coherent with the scenario suggested by the numerical simulations. Indeed, the valley is actually the crossover between the motion of the tracer inside the cage and the movement of the cage itself that enslaves the tracer. Once the presence of a persistent collective motion of the granular medium is verified, we can say that the cage moves as the collective variable on two time scales that are, with a good approximation, independent. In this picture, it is thus reasonable that the frequency (time) at which the slow component emerges in the PDS (MSD) could change independently from what is happening at the characteristic frequency (time) of the backscattering (cage) effect and vice versa. This is possible with Eqs. (10) by changing a combination of two parameters and leaving the others fixed (Fig. 6).

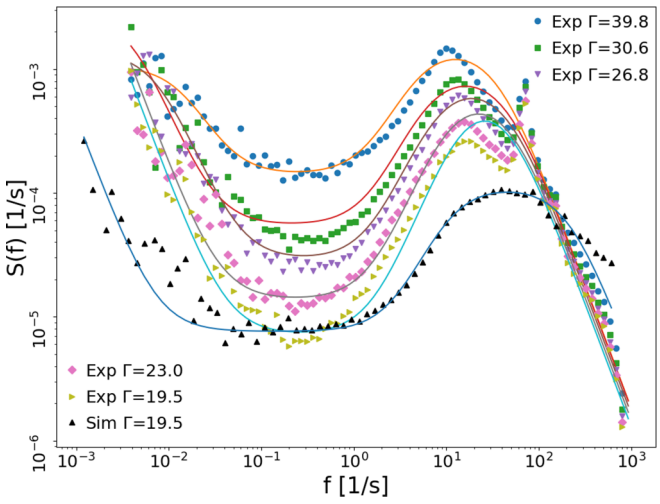

FIG. 5. Comparison between experimental/numerical data and the model [Eq. (10)] for the PDS of the tracer for many values of Γ and fixed $N = 2600$. See the caption of Fig. 2 for an explanation of the peak close to 100 Hz in the experimental spectrum.

Both for Eqs. (7) and (10), the number of independent parameters needed is actually smaller than the one used, but we have kept some redundancy for the purpose of presenting clearer model equations. Now, rescaling all the equations by the inertia I_i, we can rewrite the two models in a compact form that is more suitable for the next section. For the tracer, we have

$$\dot{\omega}(t) = -\frac{1}{\tau}[\omega(t) - \Omega(t)] + \sqrt{2\frac{q}{\tau}}\eta(t), \tag{11a}$$

$$\Omega(t) = \Omega_1(t) + \Omega_2(t), \tag{11b}$$

$$\dot{\Omega}_1(t) = -\frac{1}{\tau_1}[\Omega_1(t) + \alpha\omega(t)] + \sqrt{2\frac{q_1}{\tau_1}}\eta_1(t), \tag{11c}$$

$$\dot{\Omega}_2(t) = -\frac{1}{\tau_2}\Omega_2(t) + \sqrt{2\frac{q_2}{\tau_2}}\eta_2(t), \tag{11d}$$

where $\tau_i = I_i/\gamma_i$, $q_i = T_i/I_i$, and $\alpha = \gamma_c/\gamma_1$. Regarding the model for the collective variable alone, we note that the rescaled form of Eqs. (7) (for the granular bulk dynamics

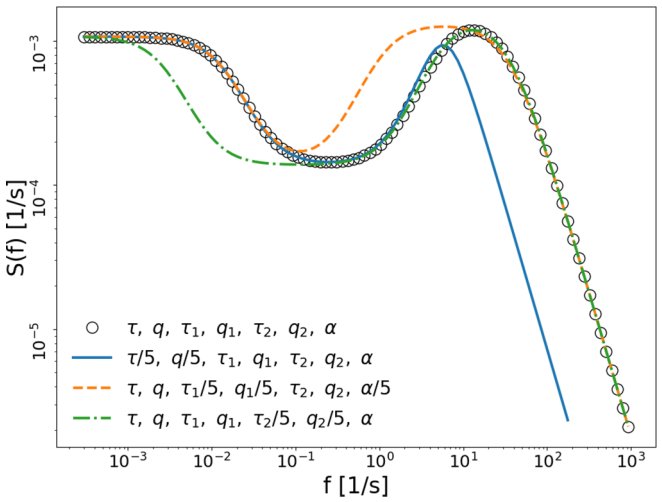

FIG. 6. Four different shapes of $S(f)$, obtained by plotting the PDS of $\omega(t)$ computed from model (10) or different arbitrary choices of the parameters where $\tau_i = I_i/\gamma_i$, $q_i = T_i/I_i$, and $\alpha = \gamma_c/I_1$. We demonstrate that it is possible to change the broadness of the valley independently of that of the backscattering peak and vice versa.

when the tracer is absent) coincides with Eqs. (11b)–(11d) once we set $\alpha = 0$.

The last aspect of the proposed model we want discuss concerns the physical meaning of couplings between variables in a system of Langevin equations. First we note that also without the introduction of auxiliary variables the effect on the tracer of the surrounding fluid is intrinsically contained in the Langevin approach. Indeed, also for ordinary Brownian motion [Eq. (11a) without $\Omega(t)$] the characteristic time τ and the stationary variance q depend on the properties of both tracer and fluid [49]. The need for additional variables emerges just in the presence of multiple time scales in the tracer dynamics. In view of this, referring to Eqs. (11), we can say that from an *energetic* point of view the effect of the granular medium on the tracer can be contained in q alone. Indeed, provided that $\tau \ll \tau_1$ and $q \gg q_1$, the fluctuations in the steady states of ω are not affected by the introduction of Ω_1. We can expect that this limit holds in our system because the inertia of the local collective variable I_1 is reasonably higher than that of the blade I. We will confirm this expectation in the next section, in which our fitting procedure shows that q and the variance of ω are almost coincident as in a single variable process.

These features are independent of α in Eq. (11c), so in this limit α represents the adimensional strength of a coupling that affects just the memory and not the energy of the tracer dynamics. In other words, the introduction of Ω_1 changes the shape of the PDS of ω leaving its integral unaltered [we remember here that if $\langle\omega\rangle = 0$, then $\int_0^\infty df\, S(f) = \langle\omega^2\rangle$]. Remarkably, studying the derivative of $S(f)$, it is possible to see that $\alpha > 0$ is a necessary condition for the occurrence of the backscattering effect. So, in our model, this effect is possible only if the tracer is coupled with a variable that is influenced by the tracer itself. This fact is compatible with the intuitive physical mechanism with which backscattering is rationalized: The surrounding fluid is perturbed by the intruder, and the latter feels with some delay in time the effect of this perturbation. In view of this mutual influence, we find even more appropriate the definition of Ω as a local field in Eqs. (10) and (11). Indeed, even if the whole granular medium can be reasonably unperturbed by the intruder, there will always be a local fraction of it that interacts reciprocally with the tracer giving rise to the backscattering effect.

This clarifies also the way in which the tracer is coupled with Ω_2 that is not affected by ω. Indeed, the cage of surrounding grains has two main effects: Confining the tracer with backscattering (coupling between ω and Ω_1 with reciprocal influence) and dragging it into the slow dynamics (coupling between ω and Ω_2 without reciprocal influence).

VI. PHYSICAL MEANING OF THE MODEL'S PARAMETERS

In this section, we attempt to systematically fit our model's parameters with the results of the numerical simulations and experiments. This task has two main motivations. First, it may suggest a way to infer or guess the model's parameters (or their behavior when physical parameters are varied) in general situations. Second, it makes more robust the identification of the model: A fuzzy or unintelligible behavior of the model's parameter would be the symptom of a weakness of the model itself.

For this purpose, we report in Table I the fitted parameters obtained for the collective variable (simulations) via Eqs. (11b)–(11d) with $\alpha = 0$ and for the tracer (experiments and simulations) via Eqs. (11) for many values of Γ. We first concentrate on the numerical data for the collective variable Ω. From Eqs. (7) and (11) it is clear that the sum of two independent OU processes depends on four parameters: τ_1, q_1, τ_2, and q_2, where τ_i is the characteristic time of the single process and q_i is its variance. In Sec. IV we verified that Eqs. (7) properly reproduce the functional form of the numerical PDS and MSD. Now we want to study how the fitted parameters behave as a function of Γ. In particular, we are interested in verifying whether their numerical values reflect the physical intuitions upon which the model with two variables is based. In Fig. 7 we can clearly see that τ_1 and q_1 are increasing with Γ while τ_2 and q_2 are decreasing. The behavior of q_1 is intuitive because we can reasonably think that this parameter grows with the "temperature" of the physical external driving (the shaker). The behavior of τ_2 and q_2 corroborates our intuition that reducing Γ induces the emergence of a slow time scale whose persistency time (τ_2) and intensity (q_2) grow. The microscopic origin of this fact can be understood by considering the dynamical heterogeneity present in this system (see, for instance, [22]): local temperature and pressure may vary a lot in space. When a collective motion emerges, we find that a great fraction of particles participates—as a condensed state—in the collective motion, and a smaller one still exhibits a gaslike behavior. We can actually imagine that the slow contribution Ω_2 to the total variable Ω is mainly due to the particles in this condensed phase, whose number could be thought of as proportional to the effective inertia of Ω_2. At this point it is clear that increasing Γ reduces the fraction of particles in the condensed phase and consequently reduces τ_2. The growth of τ_1 with Γ does not have an easy explanation in our opinion. In dilute kinetic models, the dissipative drag

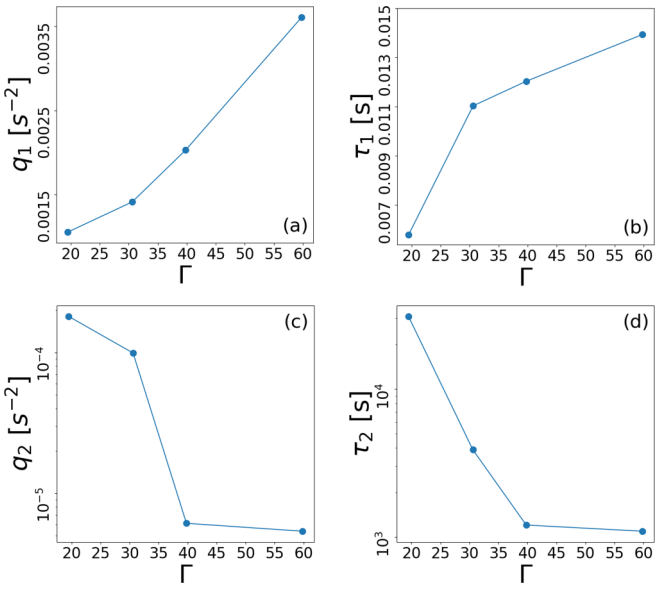

FIG. 7. Fitted parameter for the collective variable (simulations) vs Γ with fixed $N = 2600$. Fit has been done via PDS [Eq. (8b)] relative to Eqs. (11b)–(11d) with $\alpha = 0$. Numerical values of the parameters are also reported in Table I.

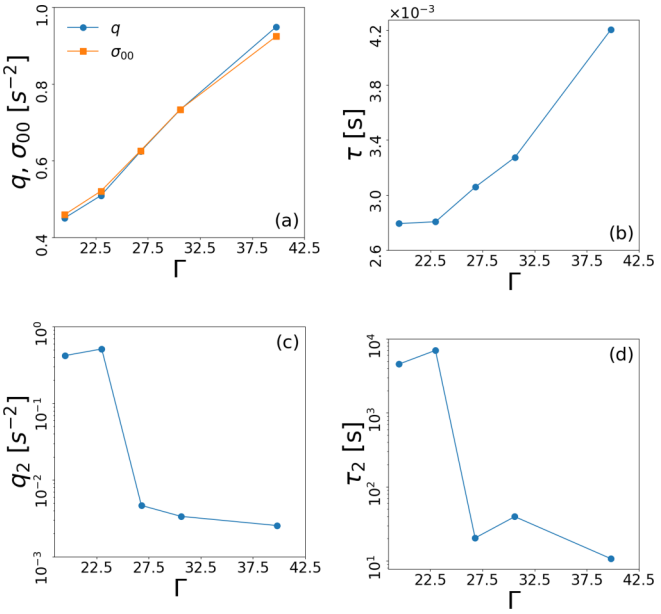

FIG. 8. Fitted parameters for experimental tracer vs Γ with fixed $N = 2600$. Fit has been done via PDS [see Eq. (A7) in the Appendix] relative to Eqs. (11). Numerical values of the parameters are also reported in Table I.

(here the inverse of τ_1) is often related to the mean collision frequency (mediated through a ratio of masses and other factors): however, this quantity may have opposite trends when Γ grows, i.e., it may increase because there is more energy (faster collisions) or it may decrease because there is a larger mean free path. Apparently, the second phenomenon dominates the first. The connection between dissipation and collision frequency, however, is reasonable for dilute gases but certainly not obvious in condensed phases.

Regarding the experimental data of the tracer, from Eqs. (11) we see that the number of free parameters for a fit is seven, and they are $\tau, q, \tau_1, q_1, \tau_2, q_2, \alpha$. We recall that q, q_1, and q_2 would be equal to the stationary variances of ω, Ω_1, and Ω_2, respectively, if these variables were not coupled. In our model with couplings one must consider the covariance matrix σ (see Appendix A 2), which is related to the noise amplitudes through a relation that also involves the coupling matrix [48]. However, in view of the discussion about couplings at the end of Sec. V, and with the aim of reducing the freedom in the fitting procedure, we decided to set q to coincide with the variance of ω measured in experiments. We then verify *a posteriori* how good is this approximation. In Fig. 8(a) we compare the experimental $\langle(\omega - \langle\omega\rangle)^2\rangle$ with the theoretical one calculated with fitted parameters, and we verify that our assumption is reasonable. The behavior of q together with that of τ, τ_2, and q_2 shown in the same figure [panels (b), (c), and (d)] is coherent with the phenomenology already explained for fast and slow parts of the collective variable of Fig. 7 (we remind the reader that Ω_2 is totally independent from the other variables, so q_2 always coincides with the variance of Ω_2). Indeed, the idea of our model is to consider the tracer (ω) enslaved by the collective variable: At short times it feels the effect of the fast component Ω_1 (high-frequency decay and backscattering peak) while at late times Ω_2 starts to dominate the entire dynamics with its persistent ballistic drifts. The motion of the tracer is then characterized by more than one characteristic time scale. Looking at Eq. (10a), it is quite natural to associate τ and q, respectively, with the characteristic time and the variance of the short-time dynamics of ω. It is therefore reassuring to find for these parameters similar behaviors to those observed for τ_1 and q_1 in numerical simulations [compare panels (a) and (b) of Figs. 7 and 8]. Also the values of τ_1 and q_1 obtained from the experimental data via Eqs. (11) (not shown in the figures but reported in Table I) follow the same qualitative behavior. Regarding couplings, our fitting procedure revealed the situation depicted at the end of Sec. V. Looking at Table I and Fig. 8, we find that the effect on the tracer of the auxiliary variables is negligible from an *energetic* point of view [$q \simeq \langle(\omega - \langle\omega\rangle)^2\rangle$] but not from a *memory* one [$\alpha \sim O(1 - 10)$ for all the fitted spectra].

The results reported in Fig. 8 regard the experimental tracer, but, as is shown for one case ($\Gamma = 19.5$) in Fig. 5, we have also tested our model on the numerical data coming from the simulations *with* the blade. We note that the good agreement shown is obtained for values of τ_1, q_1, τ_2, and q_2 that are quite different from those coming from a direct fit of the two components of the collective variable in simulations *with* or *without* the blade (see the first, second, and seventh rows of Table I). This is not surprising because, as already stated at the end of Sec. V, the variable Ω actually coupled to the tracer, in Eqs. (10) and (11), is a *local* collective variable. The latter reasonably differs—quantitatively—from the global one because of a considerable spatial heterogeneity of granular temperature and diffusivity [22].

VII. CONCLUSIONS

In conclusion, we have proposed a series of linear stochastic models to rationalize a series of experimental and numer-

ical results. In the phenomenon we have tackled, vibrofluidized dense granular materials display persistent slow drifts superimposed to fast collisional processes. We stress that the proposed models are purely phenomenological. They can be considered analogous to hydrodynamic models for dense fluids (even granular fluids), where the transport coefficients are not derived from microscopic parameters but are obtained from empirical observations. An important added value of phenomenological models for slow variables is to offer arguments in favor of the idea of scale separations, which is not always guaranteed in granular fluids [33,50,51].

We have built two main models. The first one is for the motion of the angular drift of the granular medium, which is a sum of two independent Langevin diffusions (i.e., Brownian motion with inertia), characterizing fast and slow scales: the independence is consistent with the lack of cage effects, which are usually evidence of coupling between fast and slow scales. The presence of inertia also in the slow mode provides the main ingredient for persistent ballistic motion. The second model is for the motion of a rotating tracer immersed in the granular medium, which is the most accessible variable in experiments. Such a model is built upon the idea that the tracer is coupled with a local fraction of the surrounding medium through a purely viscous interaction, similar to other granular tracer models. Since both models contain several independent parameters, it is not surprising that they reproduce all available data. Less trivial is the fact that the fitted parameters behave in a coherent way and are consistent with physical intuition, as shown in Sec. VI. We have also solved an important inconsistency of a previous model for the tracer [32], which was unable to describe the power spectrum at medium time scales.

We hope to stimulate future theoretical investigations in order to derive these models, or part of their parameters, following a kinetic theoretical approach.

ACKNOWLEDGMENTS

The authors are indebted to Marco Baldovin for fruitful scientific discussions. The authors acknowledge the financial support of Regione Lazio through the Grant "Progetti Gruppi di Ricerca" N. 85-2017-15257 and from the MIUR PRIN 2017 project 201798CZLJ.

APPENDIX: MULTIVARIATE LINEAR STOCHASTIC PROCESSES

1. Generic process with two variables

A generic multivariate linear stochastic process can be written as $\dot{X}(t) = -AX(t) + B\tilde{\eta}(t)$, where $X(t)$ is a vector of variables, $\tilde{\eta}(t)$ is a vector of white noises with zero mean and unitary variance, while A and B are the matrices that define characteristic times, diffusion coefficients, and eventually couplings of the variables. In two dimensions, assuming independent noises between the variables, we have $X(t) = \{x_0(t), x_1(t)\}$ and

$$A = \begin{pmatrix} a & b \\ c & d \end{pmatrix}, \quad B = \begin{pmatrix} D_1 & 0 \\ 0 & D_2 \end{pmatrix}, \quad \tilde{\eta}(t) = \begin{pmatrix} \eta_1(t) \\ \eta_2(t) \end{pmatrix}. \tag{A1}$$

We can now compute the spectral matrix through the following relation [48]:

$$S(f) = \frac{1}{2\pi}(A + i2\pi f)^{-1} BB^T (A^T - i2\pi f)^{-1}, \tag{A2}$$

obtaining for the spectrum of a single variable [for example $x_0(t)$]

$$S_{00}(f) = \frac{\frac{1}{2\pi}D_1^2 d^2 + 2\pi D_1^2 f^2 + \frac{1}{2\pi}D_2^2 b^2}{[16\pi^4 f^4 + 4\pi^2 f^2 (a^2 + 2bc + d^2) + a^2 d^2 - 2abcd + b^2 c^2]}. \tag{A3}$$

Computing the first derivative, we find $S'_{00}(f) = P(f)/Q(f)$, where $P(f) = c_1 f^5 + c2 f^3 + c3 f$ with $c_1, c_2 < 0$. This polynomial cannot have a double stationary point in the region $f > 0$, so there is not any choice of parameters that reproduce the behavior of interest here, i.e., a low-frequency decay followed by a backscattering peak. These results do not change if we take $x_1(t)$ instead of $x_0(t)$.

2. Model for the tracer

From Eqs. (10) we have $\dot{X}(t) = -AX(t) + B\tilde{\eta}(t)$ with $X(t) = \{\omega(t), \Omega_1(t), \Omega_2(t)\}$ and

$$A = \begin{pmatrix} \mu & -\mu & -\mu \\ \mu_1 & \alpha & 0 \\ 0 & 0 & \mu_2 \end{pmatrix}, \tag{A4}$$

$$B = \begin{pmatrix} \sqrt{2\mu q} & 0 & 0 \\ 0 & \sqrt{2\mu_1 q_1} & 0 \\ 0 & 0 & \sqrt{2\mu_2 q_2} \end{pmatrix}, \tag{A5}$$

$$\tilde{\eta} = \begin{pmatrix} \eta(t) \\ \eta_1(t) \\ \eta_2(t) \end{pmatrix}, \tag{A6}$$

where $\mu_i = 1/\tau_i = \gamma_i/I_i$, $q_i = T_i/I_i$, and $\alpha = \gamma_c/\gamma_1$. The covariance matrix σ is related to A and B through the relation $A\sigma + \sigma A^T = BB^T$. We have computed the spectrum used for the fit of Secs. V and VI always through Eq. (A2) obtaining Eq. (A7) where $\hat{f} = 2\pi f$,

$$S_{00}(\hat{f}) = \frac{\mu/\pi\left[\hat{f}^4 q + \hat{f}^2\left(\mu_1^2 q + \mu_1\mu q_1 + \mu_2^2 q + \mu_2\mu q_2\right) + \mu_1^2\mu_2^2 q + \mu_1^2\mu_2\mu q_2 + \mu_1\mu_2^2\mu q_1\right]}{\hat{f}^6 + \hat{f}^4\left(\mu_1^2 + \mu_2^2 + \mu^2 - 2\mu\alpha\right) + \hat{f}^2\left(\mu_1^2\mu_2^2 + \mu_1^2\mu^2 + 2\mu_1\mu^2\alpha + \mu_2^2\mu^2 - 2\mu_2^2\mu\alpha + \mu^2\alpha^2\right) + \mu_2^2\mu^2(\alpha + \mu_1)^2}. \tag{A7}$$

[1] H. M. Jaeger, S. R. Nagel, and R. P. Behringer, Rev. Mod. Phys. **68**, 1259 (1996).
[2] N. V. Brilliantov and T. Pöschel, *Kinetic Theory of Granular Gases* (Oxford University Press, Oxford, 2004).
[3] B. Andreotti, Y. Forterre, and O. Pouliquen, *Granular Media* (Cambridge University Press, Cambridge, 20013).
[4] A. Baule, F. Morone, H. J. Herrmann, and H. A. Makse, Rev. Mod. Phys. **90**, 015006 (2018).
[5] C. S. Campbell, Annu. Rev. Fluid Mech. **22**, 57 (1990).
[6] A. Puglisi, *Transport and Fluctuations in Granular Fluids* (Springer-Verlag, Berlin, 2015).
[7] P. Eshuis, K. van der Weele, D. van der Meer, R. Bos, and D. Lohse, Phys. Fluids **19**, 123301 (2007).
[8] G. Pontuale, A. Gnoli, F. V. Reyes, and A. Puglisi, Phys. Rev. Lett. **117**, 098006 (2016).
[9] J. J. Brey, J. W. Dufty, C. S. Kim, and A. Santos, Phys. Rev. E **58**, 4638 (1998).
[10] R. Soto, *Kinetic Theory and Transport Phenomena* (Oxford University Press, Oxford, 2016).
[11] C. Cercignani, R. Illner, and M. Pulvirenti, *The Mathematical Theory of Dilute Gases* (Springer, Berlin, 1994).
[12] V. Garzó and J. W. Dufty, Phys. Rev. E **59**, 5895 (1999).
[13] J. W. Dufty and V. Garzó, J. Stat. Phys. **105**, 723 (2001).
[14] J. P. Hansen and I. R. McDonald, *Theory of Simple Liquids* (Academic, London, 1986).
[15] D. J. Evans and G. P. Morriss, *Statistical Mechanics of Nonequilibrium Liquids* (Academic, London, 1990).
[16] A. Cavagna, Phys. Rep. **476**, 51 (2009).
[17] W. Götze, *Complex Dynamics of Glass-Forming Liquids: A Mode-Coupling Theory* (Oxford University Press, Oxford, 2008).
[18] W. T. Kranz, M. Sperl, and A. Zippelius, Phys. Rev. E **87**, 022207 (2013).
[19] W. T. Kranz, F. Frahsa, A. Zippelius, M. Fuchs, and M. Sperl, Phys. Rev. Lett. **121**, 148002 (2018).
[20] A. Gnoli, A. Lasanta, A. Sarracino, and A. Puglisi, Sci. Rep. **6**, 38604 (2016).
[21] C. Scalliet, A. Gnoli, A. Puglisi, and A. Vulpiani, Phys. Rev. Lett. **114**, 198001 (2015).
[22] A. Plati, A. Baldassarri, A. Gnoli, G. Gradenigo, and A. Puglisi, Phys. Rev. Lett. **123**, 038002 (2019).
[23] E. Ehrichs, H. Jaeger, G. S. Karczmar, J. B. Knight, V. Y. Kuperman, and S. R. Nagel, Science **267**, 1632 (1995).
[24] M. E. Möbius, B. E. Lauderdale, S. R. Nagel, and H. M. Jaeger, Nature (London) **414**, 270 (2001).
[25] N. Rivas, S. Luding, and A. R. Thornton, New J. Phys. **15**, 113043 (2013).
[26] V. Folli, N. Ghofraniha, A. Puglisi, L. Leuzzi, and C. Conti, Sci. Rep. **3**, 2251 (2013).
[27] A. Rabani, G. Ariel, and A. Be'er, PloS ONE **8**, e83760 (2013).
[28] C. Chen, S. Liu, X.-q. Shi, H. Chaté, and Y. Wu, Nature (London) **542**, 210 (2017).
[29] C.-k. Tung, C. Lin, B. Harvey, A. G. Fiore, F. Ardon, M. Wu, and S. S. Suarez, Sci. Rep. **7**, 1 (2017).
[30] C. Battle, C. P. Broedersz, N. Fakhri, V. F. Geyer, J. Howard, C. F. Schmidt, and F. C. MacKintosh, Science **352**, 604 (2016).
[31] M. Baldovin, F. Cecconi, M. Cencini, A. Puglisi, and A. Vulpiani, Entropy **20**, 807 (2018).
[32] A. Lasanta and A. Puglisi, J. Chem. Phys. **143**, 064511 (2015).
[33] M. Baldovin, A. Puglisi, and A. Vulpiani, PLoS ONE **14**, e0212135 (2019).
[34] D. Villamaina, A. Baldassarri, A. Puglisi, and A. Vulpiani, J. Stat. Mech. (2009) P07024.
[35] A. Sarracino, D. Villamaina, G. Gradenigo, and A. Puglisi, Europhys. Lett. **92**, 34001 (2010).
[36] A. Gnoli, A. Puglisi, A. Sarracino, and A. Vulpiani, PLoS ONE **9**, e93720 (2014).
[37] V. F. Sears, Proc. Phys. Soc. **86**, 953 (1965).
[38] H. D. Vollmer, Z. Phys. **33**, 103 (1979).
[39] A. Rahman, Phys. Rev. **136**, A405 (1964).
[40] S. Plimpton, J. Comput. Phys **117**, 1 (1995).
[41] H. P. Zhang and H. A. Makse, Phys. Rev. E **72**, 011301 (2005).
[42] L. E. Silbert, D. Ertas, G. S. Grest, T. C. Halsey, D. Levine, and S. J. Plimpton, Phys. Rev. E **64**, 051302 (2001).
[43] N. V. Brilliantov, F. Spahn, J. M. Hertzsch, and T. Pöschel, Phys. Rev. E **53**, 5382 (1996).
[44] Lammps Mailing List (2019), https://lammps.sandia.gov/threads/msg80848.html.
[45] Lammps Release Review (2019), https://github.com/lammps/lammps/releases/tag/stable_5Jun2019.
[46] A. Puglisi, A. Sarracino, G. Gradenigo, and D. Villamaina, Gran. Matter **14**, 235 (2012).
[47] R. Zwangzig, *Nonequilibrium Statistical Mechanics* (Oxford University Press, Oxford, 2001).
[48] C. Gardiner, *Handbook of Stochastic Methods for Physics, Chemistry and the Natural Sciences* (Springer-Verlag, Berlin, 1990).
[49] P. Langevin, C. R. Acad. Sci. (Paris) **146**, 530 (1908); translated in Am. J. Phys. **65**, 1079 (1997).
[50] I. Goldhirsch, Chaos **9**, 659 (1999).
[51] L. P. Kadanoff, Rev. Mod. Phys. **71**, 435 (1999).